

Short Communication

## Potassium Permanganate (KMnO<sub>4</sub>) Can be Employed as Anode Material for Lithium Ion Batteries

Keqiang Ding<sup>1,\*</sup>, Binjuan Wei<sup>1</sup>, Yan Zhang<sup>1</sup>, Fujuan Shi<sup>1</sup>, Chenxue Li<sup>1</sup>, Xiaomi Shi<sup>1</sup>, Junqing Pan<sup>2,\*</sup>

<sup>1</sup> College of Chemistry and Materials Science, Hebei Normal University, Shijiazhuang, Hebei 050024, P.R. China

<sup>2</sup> State Key Laboratory of Chemical Resource Engineering, Beijing University of Chemical Technology, Beijing, 100029, China

\*E-mail: [dkeqiang@263.net](mailto:dkeqiang@263.net); [jqpan@mail.buct.edu.cn](mailto:jqpan@mail.buct.edu.cn)

Received: 12 March 2017 / Accepted: 18 April 2017 / Published: 12 May 2017

For the first time, a novel finding, that potassium permanganate (KMnO<sub>4</sub>) can be directly employed as anode material for lithium ion batteries (LIBs), is reported in this short communication. To improve the electrical conductivity of KMnO<sub>4</sub>, graphene is doped into the pure KMnO<sub>4</sub> by a very simple method of milling, which leads to the formation of graphene-doped KMnO<sub>4</sub>. The samples of graphene-doped KMnO<sub>4</sub> having 1 wt. %, 2 wt.% and 3 wt.% graphene are denoted as sample a, b and c, respectively. The characteristics of the prepared samples are mainly examined by using scanning electron microscopy (SEM), cyclic voltammometry (CV), galvanostatic charge-discharge tests and electrochemical impedance spectroscopy (EIS). The results of the electrochemical measurements indicate that the discharge capacities of pure KMnO<sub>4</sub>, sample a, b and c are evaluated to be approximately 82, 92, 110 and 126 mAh g<sup>-1</sup> after 20 cycles at a current density of 100 mA g<sup>-1</sup>. This work has not only developed a novel anode material but also proposed a novel mechanism for the lithiation/delithiation process.

**Keywords:** anode material; KMnO<sub>4</sub>; graphene; electrochemical measurements; Li ion battery

### 1. INTRODUCTION

Although graphite as anode material has been successfully applied in the commercial LIBs, the lower theoretical capacity of 372 mAh g<sup>-1</sup> as well as the safety issue of graphite still greatly hampered the further applications of LIBs [1]. It is reported that the voltage of graphite is lower than the potential window of many common Li-ion battery electrolytes, thus, the electrolyte decomposition and the formation of unstable solid electrolyte interfaces (SEI) easily occurred on the surface of graphite,

which could further lead to the performance degradation of the LIBs [2]. Meanwhile, the redox potential of graphite is very close to that of the  $\text{Li}/\text{Li}^+$  couple, therefore, Li dendrite growth may take place especially when being overcharged, which may further produce cell shorting or even result in thermal runaway [3]. Thus, developing novel anode materials with high energy density, long cycle life and high rate capability has become the major challenge of the next generation of LIBs [4,5].

Till present, many kinds of anode materials have been developed with an intention to replace graphite anode material. Summarily, there are three kinds of novel anode materials. (1) Transition metal oxides (TMO) [6]. This group material can also be classified as two parts, namely, Li ions-contained TMO and Li ions-free TMO. Among the Li ion-contained TMO, lithium titanate (LTO) [7] is the most widely investigated material mainly due to its relatively higher charging/discharging voltage plateau (at around 1.55 V vs.  $\text{Li}/\text{Li}^+$ ) and the limited volume expansion/contraction during cycling. Till present, many types of Li ions-free TMO, e.g.,  $\text{Fe}_2\text{O}_3$  [8],  $\text{Co}_3\text{O}_4$  [9] and  $\text{SnO}_2$  [10], have been employed as anode materials for LIBs, showing satisfactory electrochemical performance. Careful analysis of above TMO substances revealed that the central metal atom in a TMO molecule generally has a variable valency which is the essential characteristics of this TMO group material. (2) Elementary substances. In this group, Si [11] and Sn [4] are the main typical substances that have been widely probed as potential anode materials for LIBs. However, the poor electrochemical properties of the quick capacity fading and short cycle life, which were mainly caused by the large volume change during cycles of lithiation and delithiation process, made them unsuitable for the commercial applications in LIBs. (3) Novel kinds of carbon. To improve the electrochemical properties of graphite, many kinds of carbon with novel morphologies and crystal structure, such as carbon nanotubes [12], carbon nanofiber [13] and graphene [14], have been produced recently, showing enhanced electrochemical performance as compared to the traditional anode material of graphite. Although, as mentioned above, many kinds of novel anode materials have been prepared, the complicated synthesis process and higher preparation cost have greatly limited their wide applications in the field of LIBs. Also, it is well known that except for the electrochemical properties, the preparation cost and the synthetic route are the main factors for the commercialization of a novel anode material. Or in other words, although numerous papers regarding the preparation and applications of novel anode materials are published every year, the practical applications of novel anode materials in the commercial LIBs are extremely rare. Thus, hunting for a novel anode material of LIBs is still an urgent need for the further applications of LIBs. To the best of our knowledge, the utilization of  $\text{KMnO}_4$  as anode material for LIBs has not been reported so far.

In this work, firstly, the purchased  $\text{KMnO}_4$  (denoted as sample o) was directly used as anode material for LIBs which showed unexpected electrochemical performance. To enhance the electrical conductivity of  $\text{KMnO}_4$ , graphene was doped into  $\text{KMnO}_4$  by using a very simple method of milling, showing remarkably improved electrochemical performance relative to that of pure  $\text{KMnO}_4$ . The effect of graphene content on the electrochemical performance of pure  $\text{KMnO}_4$  was thoroughly investigated through changing the content of graphene in the final samples. It should be emphasized that besides the anode material, all other parts in this work such as the counter electrode of lithium metallic foil and the electrolyte were all identical to that of the formerly reported work, thus, a brand-new mechanism of lithiation and delithiation was displayed in this work. It is believed that the novel results presented in

this preliminary work will have a huge impact on the development of anode material of LIBs, though the electrochemical properties like the discharge capacity and the cycling stability were not as good as the current anode materials.

## 2. EXPERIMENTAL

### 2.1. Materials

All chemicals were bought from Tianjin Chemical Reagent Co. Ltd. All materials used for the electrochemical testing, such as PVDF (polyvinylidene fluoride) binder, electrolyte of 1 M LiPF<sub>6</sub>, acetylene black and the cell were all supported by the Tianjin Lianghuo S&T Developing Co. Ltd. All the chemicals were used as-received without any further treatment.

### 2.2. Preparation of graphene-doped KMnO<sub>4</sub>

1 g KMnO<sub>4</sub> and 0.01 g graphene were thoroughly mixed for 5 min, and then the resultant mixture was milled in an agate mortar for 10 min to prepare the 1 wt.% graphene doped KMnO<sub>4</sub>, which was denoted as sample a. Similarly, other samples were fabricated using the same process. Briefly, the as-prepared graphene-doped KMnO<sub>4</sub> containing 1wt.%, 2 wt.% and 3 wt.% graphene are denoted as sample a, b and c, respectively. KMnO<sub>4</sub> was directly employed as anode material only after a 10 min milling, which was nominated as sample o.

### 2.3. Characterization

The particle morphology was observed by scanning electron microscopy (HITACHI, SEM S-570). Energy dispersive spectrometer (EDS, INCA Energy 350, England) was employed to analyze the components of the as-prepared samples.

Electrochemical measurements were performed on a CHI 660B electrochemical workstation (Shanghai Chenhua Apparatus, China) which was controlled by a personal computer. In the electrochemical impedance spectroscopy (EIS) measurement, the frequency of the alternating current (AC) employed was from 0.1 Hz to 100 kHz, and the oscillation voltage applied to the cells was 5 mV. All reported experiments in this communication were carried out at room temperature.

Prior to the preparation of the working electrode, the active material slurry was made first. Namely, the as-prepared samples, acetylene black and PVDF (polyvinylidene fluoride) binder were blended together at a weight ratio of 8:1:1 to produce a mixture. Subsequently, several drops of N-methylpyrrolidone were dropped into the resultant mixture, and then, the active material slurry was prepared after a thorough 10 min stirring. And then, the slurry was uniformly pasted onto a Cu foil using a glass piece and dried at 120 °C for 6 h in a vacuum oven, leading to the formation of a working electrode. The half battery consisting of a lithium metal foil and the synthesized working electrode was assembled in a high pure nitrogen-filled glove box. It should be noted that Celgard 2400 separator and an electrolyte of 1 M LiPF<sub>6</sub> in a mixed solvent having ethylene carbonate (EC) and diethyl carbonate

(DEC) and dimethyl carbonate (DMC) (2:5:11, vol.) were utilized in the preparation of half batteries. Evidently, the metallic lithium foil was utilized as both the reference and counter electrodes. The galvanostatic charge-discharge tests were carried out on a battery testing system (CT-3008W-5V20mA-S4, Shenzhen Neware Electronics Co., Ltd. China). In this preliminary work, the current density and the potential range were  $100 \text{ mA g}^{-1}$ , and 0~4V, respectively.

### 3. RESULTS AND DISCUSSION

#### 3.1 Characterizations of the samples

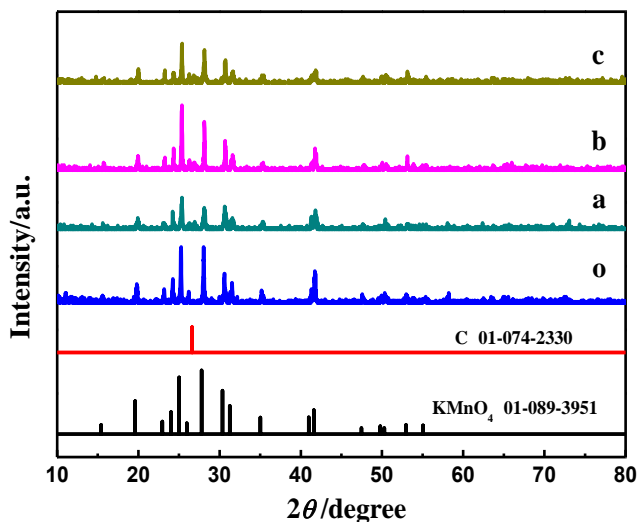


**Figure 1.** XRD patterns of all the synthesized samples. Patterns o, a, b and c correspond to sample o, a, b and c.

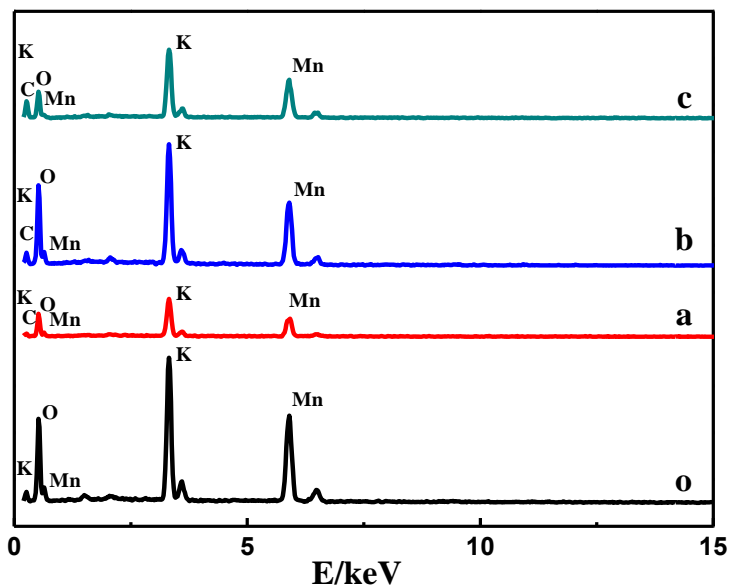


**Figure 2.** EDS spectra for all the samples. Curves o, a, b and c correspond to sample o, a, b and c.

XRD patterns of all the prepared samples as well as the standard XRD patterns of  $\text{KMnO}_4$  are well presented in Fig.1. Apparently, the main diffraction peaks assigned to  $\text{KMnO}_4$  are well exhibited

in all obtained XRD patterns, which confirmed that the starting material was  $\text{KMnO}_4$  rather than other substances. Meanwhile, the small diffraction peaks appearing at  $26.6^\circ$  should be assigned to the (002) facet of graphene basing on our previous work concerning graphene [15]. It effectively demonstrated that graphene was really doped into the final samples.

The compositions of the samples were also examined by EDS analysis. The typical results are plotted in Fig.2. For the pure  $\text{KMnO}_4$  (curve o), the peaks corresponding to K, Mn and O were all clearly exhibited. Moreover, the atomic ratio of K: Mn: O was 1:1:4, further confirming that the starting material was  $\text{KMnO}_4$  and no other impurities were introduced. While, for the graphene-doped  $\text{KMnO}_4$ , the peak of C element was detected, and the atomic ratio of K: Mn: O still remained unchanged. The results of Fig.1 and Fig.2 substantially demonstrated that graphene was really doped into the pure  $\text{KMnO}_4$  and no novel substances were created in the prepared samples.

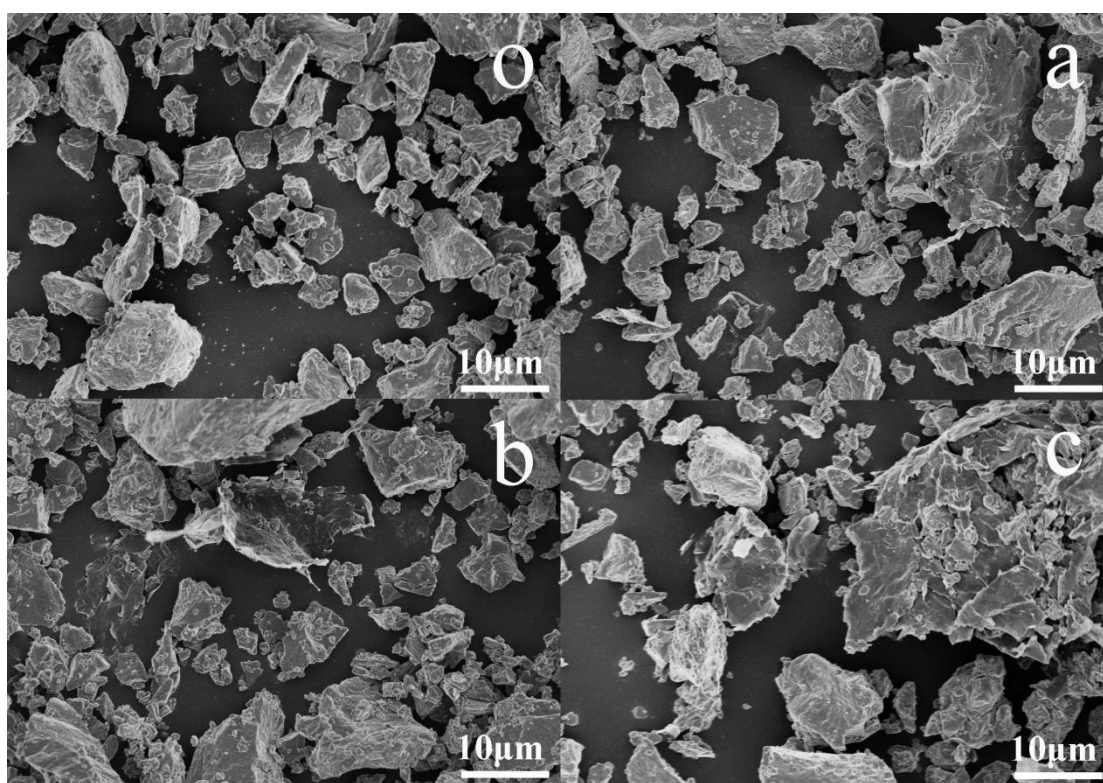


**Figure 3.** SEM images for all the samples. Images o, a, b and c correspond to sample o, a, b and c.

SEM images of the as-prepared samples are displayed in Fig.3. It is evident that for the pure  $\text{KMnO}_4$ , particles with irregular shapes were observed. Also, it can be seen that the particle size of pure  $\text{KMnO}_4$  ranged from  $1\mu\text{m}$  to  $10\mu\text{m}$  and each particle had many edges. While for sample a, b and c, except for the appearance of sheets of graphene, no evident difference in morphologies for the resultant samples was found. That is to say, no special morphology was created in the synthesized samples and all the electrochemical performances displayed by the samples should be determined by their nature.

## 3.2 Electrochemical properties

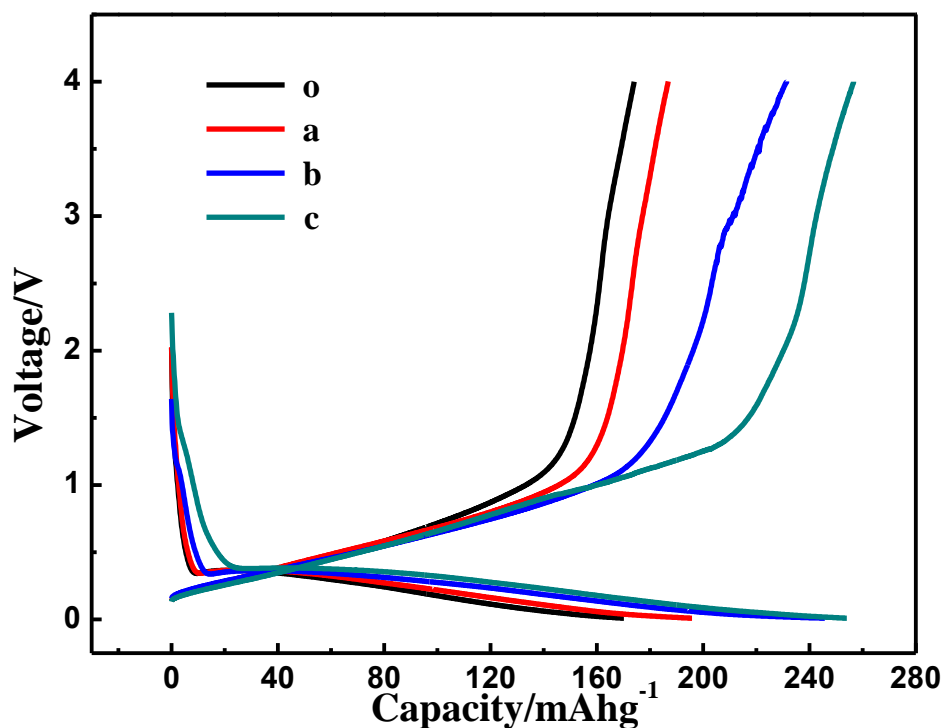


**Figure 4a.** The initial galvanostatic charge-discharge curves at the current density of  $100 \text{ mA g}^{-1}$  in the potential range of 0-4 V. Curve o, a, b and c corresponded to half-cells assembled by sample o, a, b and c.

Fig.4a shows the initial charge-discharge profiles measured in the potential range of 0-4 V at a current density of  $100 \text{ mA g}^{-1}$  for all the samples. Apparently, slightly sloped voltage plateaus are observed for each half cell during the charge and discharge processes. It strongly indicated that the delithiation and lithiation process could well proceed in all prepared materials. That is to say, all prepared samples can be utilized as anode materials for LIBs. To the best of our knowledge, this is the first time to report the delithiation and lithiation process of  $\text{KMnO}_4$ . The initial discharge capacities for sample o, a, b and c were estimated to be approximately 170, 196, 245 and 253  $\text{mAh g}^{-1}$ , respectively. It should be noted that the discharge capacity of  $170 \text{ mAh g}^{-1}$  for the pure  $\text{KMnO}_4$  was very close to the theoretical discharge capacity of lithium titanate (LTO,  $1\text{C}=175\text{mAh g}^{-1}$ ) [16]. Apparently, the discharge capacities for the graphene-doped  $\text{KMnO}_4$  samples were all remarkably larger than that of the pure  $\text{KMnO}_4$ , which can be mainly attributed to the enhanced electrical conductivity of  $\text{KMnO}_4$  by the doped graphene. Also, it should be emphasized that the discharge voltage plateau of all the samples (about 0.36V vs.  $\text{Li/Li}^+$ ) was markedly lower than that of LTO (around 1.5V vs.  $\text{Li/Li}^+$ ), which meant that the output voltages of the cell assembled by the prepared samples should be higher than that constructed by LTO when employing both identical cathode materials and electrolyte.

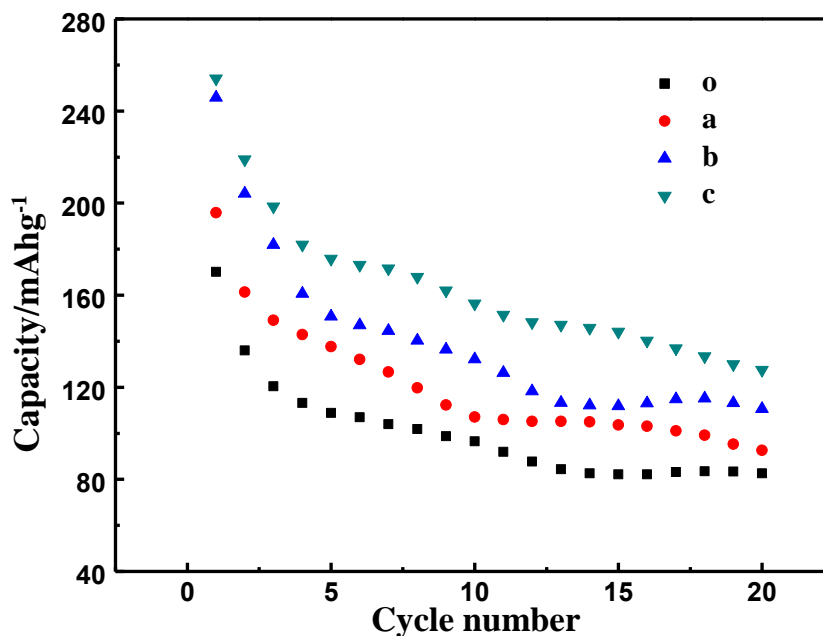


**Figure 4b.** Cyclic performance for all prepared batteries at the current density of  $100 \text{ mA g}^{-1}$ . Curve o, a, b and c correspond to half-cells assembled by sample o, a, b and c.

The cycling performances for all prepared materials are shown in Fig. 4b. It can be seen that for all the samples, the discharge capacities decreased slightly with increasing the cycle number, which was a common phenomenon since all the practical processes were the irreversible processes. Obviously, all the graphene-doped  $\text{KMnO}_4$  samples showed much higher discharge capacity than the pure  $\text{KMnO}_4$ , which indicated that the doping of graphene could greatly promote the electrochemical performance of  $\text{KMnO}_4$ . The discharge capacities of the first cycle for sample o, a, b and c were 170, 196, 245 and 253  $\text{mAh g}^{-1}$ , respectively. And at the 20<sup>th</sup> cycle, the discharge capacities for the sample o, a, b and c were estimated to be 82.9, 91.6, 110.7 and 126.2  $\text{mAh g}^{-1}$ , which were equal to 48.7%, 46.7%, 45.2% and 49.9% of their initial discharge capacities, respectively. It seemed that more amounts of doped graphene in pure  $\text{KMnO}_4$  were favorable for the enhancement of electrochemical performance of  $\text{KMnO}_4$ . Evidently, the enhancement of graphene amount would inevitably increase the preparation cost of a lithium ion battery, which was not advantageous to the large scale production of LIBs. The research work concerning the optimum content of graphene in the graphene-doped  $\text{KMnO}_4$  was under progress in our lab.

Cyclic voltammetry (CV) technique was also employed, desiring to further understand the mechanism of redox reactions in the charge-discharge processes, to examine the electrochemical behaviors of the prepared half batteries. To simplify, cyclic voltammograms (CVs) of sample o and a are illustrated in Fig.5. It is seen clearly that for the pure  $\text{KMnO}_4$  the redox peaks assigned to the delithiation and lithiation process were too weak to be visible. Interestingly, two pairs of redox peaks were exhibited definitely in the sample a-constructed half battery. It effectively demonstrated that the doping of graphene could significantly enhance the kinetics of delithiation and lithiation process in  $\text{KMnO}_4$ . Generally, the oxidation peak corresponded to the delithiation process of an anode material, and the reduction peak was closely related to the lithiation process of an anode material.

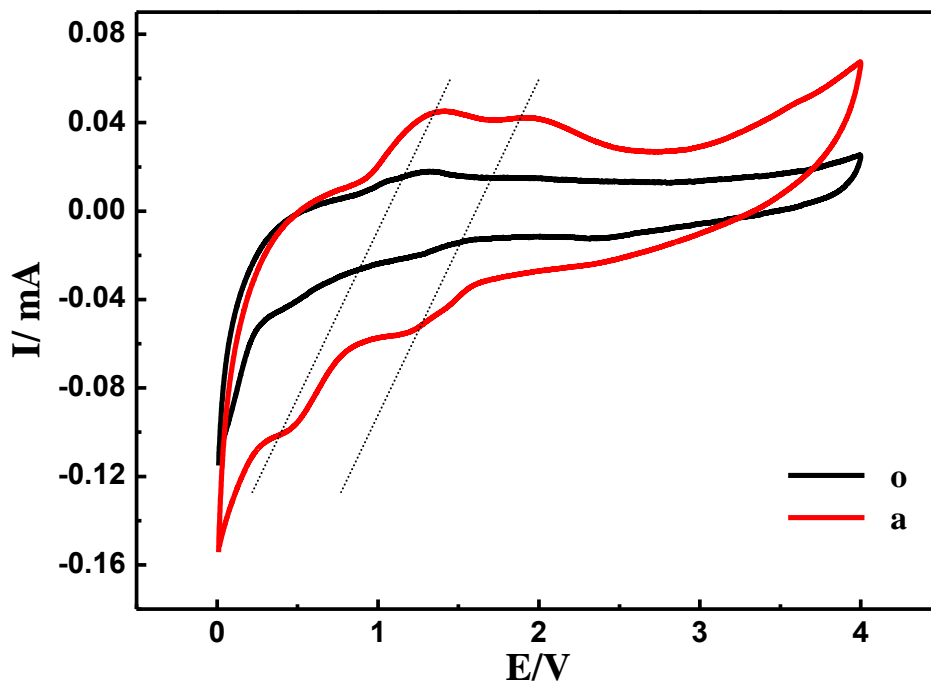
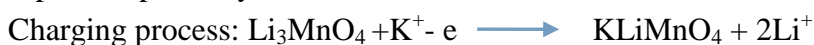


**Figure 5.** Cyclic voltammetry curves at a scan rate of  $1 \text{ mV s}^{-1}$  in the potential range of 0-4 V. Curve o and a correspond to the half-cell assembled by sample o and a.

It should be noted that the half-cell was first discharged at a current density of  $100 \text{ mA g}^{-1}$ , and then the charging process was followed which was recorded as the initial curve in Fig.4a. That is to say, the charging curve was measured first and then the discharging curve was plotted. Probably, after the initial discharging process,  $\text{KMnO}_4$  was totally converted into  $\text{Li}_3\text{MnO}_4$  [17] under the driving forces from the external power and concentration diffusion, thus, the following delithiation and lithiation process probably occurred in  $\text{KMnO}_4$ .



That is to say, in the first step of charging process, the oxidation state of Mn in  $\text{Li}_3\text{MnO}_4$  was converted from +5 to +6 which was accompanied by the incorporation of  $\text{K}^+$  and the extraction of  $\text{Li}^+$ , and in the second step of charging process,  $\text{KMnO}_4$  was reproduced which was followed by the oxidation state variation from +6 to +7 and the extraction of  $\text{Li}^+$ . And, in the discharging process, the opposite delithiation and lithiation processes probably occurred, which led to the formation  $\text{Li}_3\text{MnO}_4$ . As a result, two pairs of redox peaks were observed in the CV curves as shown in Fig. 5. Of course, above mechanism of delithiation and lithiation process was only a conjecture which was mainly deduced from the results shown in Fig.5. Obviously, the voltage plateau should be above 2.0V if only  $\text{Li}^+$  was involved in the charging-discharging process described above [18]. Or in other words, Li-Mn-O system has been widely investigated as cathode material which has a higher voltage plateau in the charging-discharging curves [19, 20]. In this work, a new system that contained  $\text{KMnO}_4$  and  $\text{LiPF}_6$  and

organic solvent was created, which was rather different from the previously reported system concerning LIBs. Therefore, there must be a novel mechanism for interpreting the charging-discharging mechanism presented in this work. More works are really required for achieving satisfactory explanation.

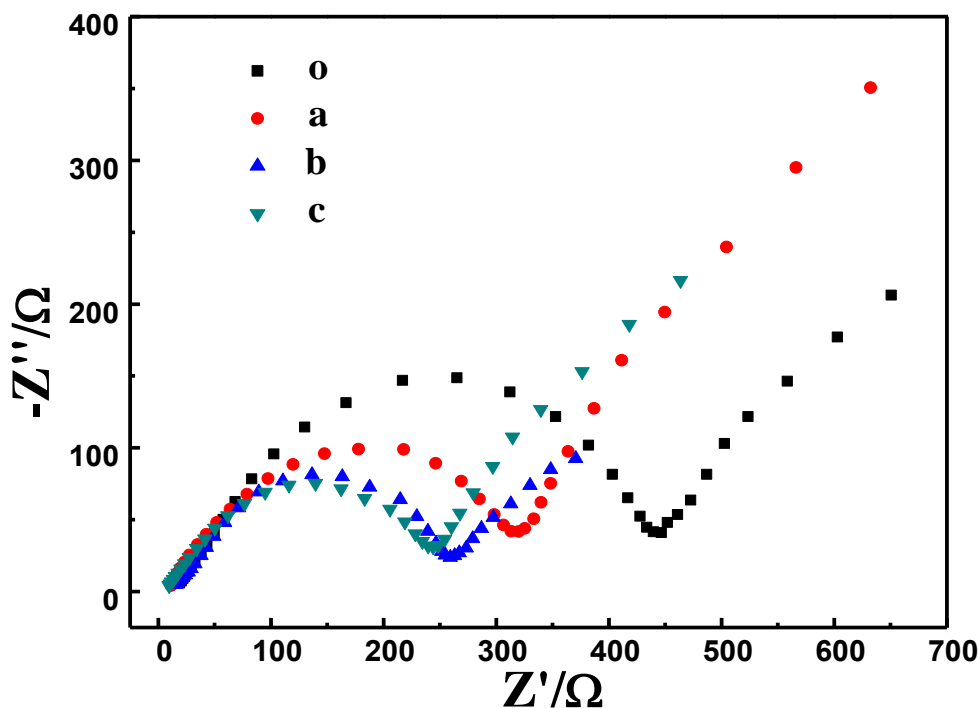


**Figure 6.** Impedance spectra (Nyquist plot) of all prepared batteries. Curve o, a, b and c correspond to the half-cells assembled by sample o, a, b and c.

Electrochemical impedance spectroscopy (EIS) as a conventional method has been widely used in investigating the electrochemical performance of a lithium ion half battery mainly because of its simple analysis [21]. Nyquist plot, as one typical curve in EIS, is the most widely used plot from which the electrochemical performances of different Li half-cells can be easily analyzed and compared. Fig. 6 gives Nyquist curves of all the synthesized half cells. It should be mentioned that these curves in Fig.6 were recorded after 20 cycles testing and all the curves were measured at their open circuit potentials. Generally, for a typical Li half-cell, the total resistance (Ohmic resistance ( $R_{\Omega}$ )) of the electrolyte, separator, and electrical contacts was presented by the intercept at the  $Z'_{real}$  axis in highest frequency region. The sloped line in the low frequency region, which was generally associated with lithium-ion diffusion in an electrode material, corresponded to the Warburg impedance [21]. The depressed semicircle in the high-middle frequency range was originated from the charge transfer resistance ( $R_{ct}$ ). Among above parameters,  $R_{ct}$  was the most valuable parameter that can be used to compare the kinetics of an electrode reaction directly. Also, the value of  $R_{ct}$  was approximately equal to the diameter of the semicircle appearing in the high-middle frequency region. Thus, the values of  $R_{ct}$  for sample o, a, b and c were estimated to be 470  $\Omega$ , 345  $\Omega$ , 278  $\Omega$  and 251  $\Omega$ , respectively. It strongly indicated that the doped graphene could markedly accelerate the lithium insertion/extraction velocity, generating a faster

kinetics as compared to pure  $\text{KMnO}_4$ . The results shown in Fig.6 were consistent with those consequences displayed in Fig.4a.

#### 4. CONCLUSIONS

For the first time, the purchased  $\text{KMnO}_4$  was directly employed as anode material for LIBs, showing a discharge capacity of  $82 \text{ mAh g}^{-1}$  after 20 cycles at the current density of  $100 \text{ mA g}^{-1}$ . This result was an amazing result since it meant that a novel group materials, namely,  $\text{KMnO}_4$ -based anode material, was found. This novel finding probably could greatly reduce the preparation cost of anode materials. Also, in this preliminary, three kinds of graphene-doped  $\text{KMnO}_4$  were produced by a very simple method of milling. As expected, the significantly enhanced electrochemical performances were exhibited by the graphene-doped  $\text{KMnO}_4$  as compared to the pure  $\text{KMnO}_4$ . Additionally, a  $\text{K}^+$  and  $\text{Li}^+$  involved mechanism of lithiation and delithiation process was proposed which may roughly explain the electrochemical performance shown by the prepared samples, basing on the CV curves obtained. It is expected that this pioneering work may not only start the research work of  $\text{KMnO}_4$ -based anode materials but also may bring about brand-new mechanism, namely,  $\text{K}^+$  and  $\text{Li}^+$  involved mechanism for explaining lithiation and delithiation process.

#### ACKNOWLEDGEMENTS

This work was financially supported by National Natural Science Foundation of China (No. 21676022 & 21173066), the State Key Program of National Natural Science of China (21236003), Natural Science Foundation of Hebei Province of China (No. B2011205014 and B2015205150), the Fundamental Research Funds for the Central Universities (JD1612 and YS1406), BUCT Fund for Disciplines Construction and Development (No. XK1531).

#### References

1. X. Lu, L. Gu, Y.-S. Hu, H.-C. Chiu, H. Li, G. P. Demopoulos and L. Chen, *J. Am. Chem. Soc.*, 137 (2015)1581.
2. B. Wang, Z. Wen, J. Jin, X. Hong, S. Zhang and K. Rui, *J. Power Sources*, 342 (2017) 521.
3. P. Li, S. Qian, H. Yu, L. Yan, X. Lin, K. Yang, N. Long, M. Shui and J. Shu, *J. Power Sources*, 330 (2016) 45.
4. Z. Yi, Q. Han, D. Geng, Y. Wu, Y. Cheng and L. Wang, *J. Power Sources*, 342 (2017) 861.
5. Y. Deng, C. Fang and G. Chen, *J. Power Sources*, 304 (2016) 81.
6. Z. Wang, L. Zhou and X. W. Lou, *Adv. Mater.*, 24 (2012) 1903.
7. Q. Zhang, M. G. Verde, J. K. Seo, X. Li and Y. Shirley Meng, *J. Power Sources*, 280 (2015) 355.
8. Y. Huang, Z. Lin, M. Zheng, T. Wang, J. Yang, F. Yuan, X. Lu, L. Liu and D. Sun, *J. Power Sources*, 307 (2016) 649.
9. L. Li, G. Zhou, X.-Y. Shan, S. Pei, F. Li and H.-M. Cheng, *J. Power Sources*, 255 (2014) 52.
10. R. Liu, D. Li, C. Wang, N. Li, Q. Li, X. Lü, J. S. Spendelov and G. Wu, *Nano Energy*, 6 (2014) 73.
11. H. Tian, X. Tan, F. Xin, C. Wang and W. Han, *Nano Energy*, 11 (2015) 490.
12. X. Yue, W. Sun, J. Zhang, F. Wang and K. Sun, *J. Power Sources*, 329 (2016) 422.
13. L. Zhang, G. Lin Xia, Z. Guo, D. Sun, X. Li and X. Yu, *J. Power Sources*, 324 (2016) 294.
14. X. Tian, Y. Zhou, X. Tu, Z. Zhang and G. Du, *J. Power Sources*, 340 (2017) 40.

15. K. Ding, Y. Zhao, L. Liu, Y. Li, L. Liu, L. Wang, X. He and Z. Guo, *Electrochim. Acta*, 176 (2015) 240.
16. K. Ding, J. Zhao, J. Zhou, Y. Zhao, Y. Chen<sup>1</sup>, Y. Zhang, B. Wei, L. Wang and X. He, *Int. J. Electrochem. Sci.*, 11 (2016) 446.
17. J. A. Saint, M. M. Doeff and J. Reed, *J. Power Sources*, 172 (2007) 189.
18. S. Soiron, A. Rougier, L. L. Aymard and J-M. Tarascon, *J. Power Sources*, 97-98(2001)402.
19. W.P. Kilroy, W.A. Ferrando and S. Dallek, *J. Power Sources*, 97-98(2001) 336.
20. G. Jin, H. Qiao, H. Xie, H. Wang, K. He, P. Liu, J. Chen, Y. Tang, S. Liu and C. Huang, *Electrochim. Acta*, 150 (2014) 1.
21. K. Ding, H. Gu, C. Zheng, L. Liu, L. Liu, X. Yan, Z. Guo, *Electrochim. Acta*, 146 (2014) 585.

© 2017 The Authors. Published by ESG ([www.electrochemsci.org](http://www.electrochemsci.org)). This article is an open access article distributed under the terms and conditions of the Creative Commons Attribution license (<http://creativecommons.org/licenses/by/4.0/>).